Influence of multiple flexible flagella on the flagellar propulsion of spermatozoa

J. Leeftink

University of Twente, Faculty of Engineering Technology - Biomechanical Engineering, Drienerlolaan 5, 7522 NB, Enschede, The Netherlands
j.leeftink@student.utwente.nl

ABSTRACT: The beat pattern of spermatozoa can be described by three wave variables; the mean flagellar curvature, the amplitude rise and the wavelength. Using high-speed videoscopy, sperm cells with one and two flagella in different viscosities are analyzed. Using the obtained data, the average wave variables and velocities were studied. It was found that double flagellar sperm cells have a higher flagellar propulsion than single flagellar sperm cells at high viscosities. Additionally, it was found that the wave variables at high viscosities are lower than the wave variables at low viscosities. Using regularized stokeslets, the flowfields around the flagella are obtained. It is observed that the flowfield around flagella always consists out of a repulsive field along the long axis of the sperm cell and an attractive field along the sides of the sperm. For double flagellar sperm cells, it is found that the flagellar propulsion is increased as long as the flagella beat in a synchronized pattern. Furthermore, the wave variables of both flagella should be similar. This amplifies the flagellar propulsion and generates a greater thrust.

Key words: flagellar propulsion, Resistive Force Theory, microrobotics, spermbots, wave variables, spermatozoa, regularized stokeslets

1 INTRODUCTION

Minimally invasive medicine is an uprising technology within healthcare. Minimally invasive medicine can reduce costs of treatments, post-surgery pain, risk of infections and the recovery time. It can be used for multiple therapeutic tasks within the human body, for example; targeted drug delivery, telemetry, biopsy, etc.[1] A division can be made in tethered and untethered robots. Untethered robots on microscale could access complex and small regions within the human body that are not accessible to tethered robots. Regions such as gastrointestinal, brain, spinal cord, blood capillaries and inside the eye could be accessed while being minimally invasive [2]. The possibility of untethered robots brings about major patient-benefits. In order to improve this field of medicine, research has to be performed on multiple fields. One of these fields being soft microrobots.

Within the human body, the propulsion of soft microrobots introduces a problem. The Reynolds number is very low which makes propulsion at small scales hard [3]. In nature, this problem is overcome by a micro motor operated flagellum which can be found in bacteria, microalgae, spermatozoa, etc. Among these cells, spermatozoa are considered to generate a relatively large thrust [4]. For minimally invasive medicine, spermatozoa are of great value due to their flagellar propulsion and natural power source. Therefore, it is of great value to mimic or use the efficient flagellar propulsion exerted by sperm cells. A spermatozoa being used as part of a biohybrid soft microrobot is called a spermbot. Within the human body, some flows have a strong current and are currently impassable by soft microrobots. Think of the circulatory system; the soft microrobot should overcome the pulsating flow of blood, which is of great strength when one thinks of the size of microrobots. In order to overcome strong currents, the flagellar propulsion of soft microrobots should be increased. Intuitively, one would add a second flagella to the robot to increase its thrust. However, the effects of a second flagella is yet unknown. This paper will study the effect of multiple flagella on the flagellar wave propulsion and their hydrodynamic interaction.

The remainder of this thesis is organized as follows: Section (2) includes the methodology and the theory around soft microrobots and flagella and Section (3), shows the results of this research.

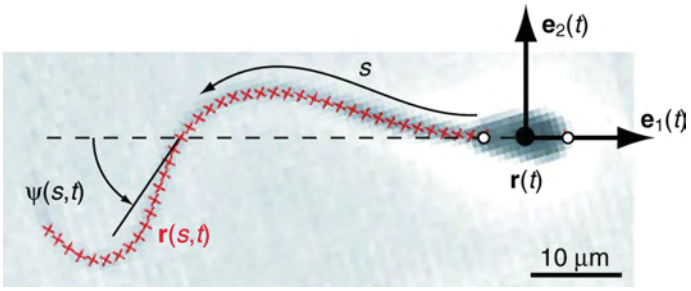

Fig. 1: A bull sperm at a specific moment in time with the position vector $r(s,t)$ in red. $e_1(t)$ is the unit vector along the long axis of the sperm head. $e_2(t)$ is the unit vector orthogonal to $e_1(t)$. The arc length s is the length along the flagellum ranging from $0 < s < L$. The tangent angle $\psi(s,t)$ is the angle between $e_1(t)$ and the tangent of the flagellum [5].

2 METHODOLOGY

2.1 Wave characteristics

Using high-speed videoscopy, videos are obtained containing images of bullsperm trapped near a flat surface. Using these videos, the sperm cells can be tracked and the flagellar motion can be analyzed. Since the sperm cells are trapped near a flat surface, the beat patterns can be assumed planar. The shape of the flagellum can be described by the position vector $r(s,t)$, where s is the arc length and t is time, as follows:

$$r(s,t) = {}^{i}r(t) - a^{i}e_1(t) - \int_0^s \cos^{i}\psi(v,t)^{i}e_1(t) + \sin^{i}\psi(v,t)^{i}e_2(t)\mathrm{d}v. \quad (1)$$

In Equation (1), $e_1(t)$ is the unit vector along the long axis of the sperm head, $e_2(t)$ is the unit vector orthogonal to $e_1(t)$ and $\psi(s,t)$ is the tangent angle as can be seen in Figure (1). The tangent angle can be described as:

$$\psi(s,t) = K_0 s + 2A_0 s \cos\left(\omega t - \frac{2\pi s}{\lambda}\right), \quad (2)$$

where K_0 is the mean flagellar curvature, A_0 is the amplitude rise, ω is the angular velocity and λ is the wavelength. Every flagellar wave can be described by K_0, A_0 and λ, which are called the wave variables. These wave variables can be obtained using the Fourier series describing the flagellar beat as follows:

$$\psi(s,t) \approx \tilde{\psi}_0(s) + \tilde{\psi}_1(s)e^{i\omega t} + \tilde{\psi}_1^*(s)e^{-i\omega t}, \quad (3)$$

where * denotes the complex conjugate of the Fourier mode. In Equation (3), only the first and second Fourier modes are considered since they contribute for 95% to the total beat power [6]. From the above equations, the wave variables can be obtained [5]. These variables can be described as the following:

$$\tilde{\psi}_0(s) = K_0 s, \quad (4)$$

$$\left|\tilde{\psi}_1(s)\right| = A_0 s, \quad (5)$$

$$-\arg\tilde{\psi}_1^*(s) = \phi(s) = \frac{2\pi s}{\lambda}. \quad (6)$$

Using MATLAB, the wave variables can be extracted from the videos. First, the shape of the flagellum is obtained from the videos frame by frame. This is done by tracking the tail with multiple points. These points are then connected using a polynomial. With this polynomial, and the equations above, the wave variables can be obtained [7]. Figure (2) shows a schematic of a double flagellar sperm cell together with an experimental sample. The red dots depict the multiple points through which the polynomial will be fit.

For every sample, the wave variables are obtained for the duration of three beat cycles. The variables for every beat cycle are averaged to get accurate variables.

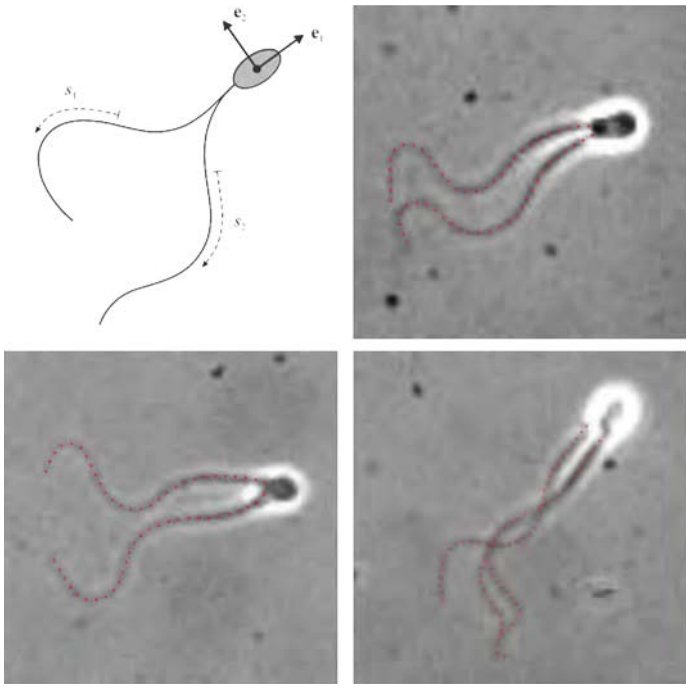

Fig. 2: A schematic of a double flagellar sperm cell where s_1 is the arc lenght of the first tail and s_2 is the arc lenght of the second tail. The sperm head is modelled as a rigid elipsoid.

2.2 Flagellar propulsion

In order to find the force exerted by the flagellum, the resistive force theory (RFT) by J. Gray and J. Hancock [8] is used. The RFT subdivides the flagellum into multiple infinitesimal elements. Over these elements, the drag and thrust force are calculated. Using superposition, the total force can be determined. Using MATLAB, the RFT can be applied. Using the wave variables K_0, A_0 and λ, the wave can be described. Subsequently, the force can be obtained using the following equation:

$$\delta F = \delta N \sin\theta - \delta L \cos\theta, \tag{7}$$

where δN and δL are the reactions from the water acting normally and tangentially to the surface of the element. δN and δL are given by:

$$\delta N = C_N \left(V_y \cos\theta - V_x \sin\theta\right) \delta s, \tag{8}$$

$$\delta L = C_L \left(V_y \sin\theta + V_x \cos\theta\right) \delta s, \tag{9}$$

where δs is a short element, θ is the angle between $e_1(t)$ and the tangent of the element, V_x is the velocity in the direction of $e_1(t)$ and V_y is the velocity in the direction of $e_2(t)$. C_N and C_L are the normal and tangential coefficients of resistance, respectively. The resultant forward thrust can be described as follows:

$$\delta F = \frac{\left(C_N - C_L\right) V_y \tan\theta - V_x \left(C_L + C_N \tan^2\theta\right)}{1 + \tan^2\theta} \delta s. \tag{10}$$

It is known that $\tan\theta = dy/dx$ and $V_y = dy/dt$. Furthermore, when θ is assumed to be small, $\tan^2\theta$ can be considered zero. This gives the following equation for the propulsive force:

$$dF = \left\{ \frac{\left(C_N - C_L\right) \frac{dy}{dt}\frac{dy}{dx} - V_x \left[C_L + C_N \left(\frac{dy}{dx}\right)^2\right]}{I + \left(\frac{dy}{dx}\right)^2} \right\} ds, \tag{11}$$

The tangential drag coefficient can be described as:

$$C_L = -\frac{2\pi\mu}{\left(\log\frac{d}{2\lambda}\right) + \frac{1}{2}}, \tag{12}$$

and the normal coefficient of resistance $C_N = 2C_L$. Integrating Equation (11) over s gives the total force exerted by the flagellum per beat cycle [8]. Using the computational power of MATLAB, the forces exerted by the different flagella can be calculated.

2.3 Fluid response using regularized stokeslets

As a means to get a better insight into the flagellar propulsion of sperm cells, the flow field is of interest. In order to obtain the flow field, the sperm cell should be modeled. This can be done by plotting a circular head of radius 3 μm together with a tail of length L_{tail} as described by Friedrich [5]. This tail consists out of infinitesimal filaments. On these filaments, the theory of regularized stokeslets [9] [10] [11] can be applied:

$$\begin{aligned}\mathbf{u}(x) = \sum_{i=1}^{M}\sum_{k=1}^{N} \frac{-{}^{i}F_k}{4\pi\eta}\left[\ln\left(\sqrt{r_k^2+\epsilon^2}+\epsilon\right) - \epsilon X\right] \\ + \frac{1}{4\pi\eta}\left[{}^{i}\mathbf{F}_k \cdot \left(\mathbf{x} - {}^{i}r_k\right)\right]\left(\mathbf{x} - {}^{i}r_k\right) X,\end{aligned} \tag{13}$$

where X is given by:

$$X = \frac{\left(\sqrt{r_k^2+\epsilon^2}+2\epsilon\right)}{\left(\sqrt{r_k^2+\epsilon^2}+\epsilon\right)^2 \sqrt{r_k^2+\epsilon^2}}. \tag{14}$$

In Equation (13), $u(x)$ is the fluid response. Furthermore, $r_k = |x - {}^{i} r_k|$ describes the distance between x and the source ${}^{i}r_k$ of the ith filament. The centerline of the flagellum can be represented as in Equation (1). With Equations (1) and (2), the total kinematics of the flagellum is described. Together with Equation (13), the flow field around the flagellum can be described. Using MATLAB, the flowfield around one or multiple flagella can be computed based on the wave variables.

3 RESULTS

3.1 A statistical observation

Multiple sperm cells were analyzed using the method described in Section (2.1). In total, 10 single flagellar and 13 double flagellar sperm cells were analyzed, resulting in a total of 34 flagella. All data was collected and used as a first insight into the behaviour of sperm cells. Since the wave variables differ for every sample and situation, it is of importance to determine the mean and standard deviation of these variables. The mean μ and standard deviation σ are determined using:

$$\mu = \frac{\sum_{i=1}^{n} x_i}{n}, \tag{15}$$

and

$$\sigma = \sqrt{\frac{\sum_{i=1}^{n}(x_i - \mu)^2}{n}}, \tag{16}$$

where n is the amount of samples and x_i is the ith wave variable.
It was found that the mean of the averaged path velocity of single flagellar sperm cells is 97.02 (± 25.63) µm/s. For sperm cells with two flagella, the mean of the averaged path velocity is 84.17 (± 32.96) µm/s. If the mean and standard deviation are taken for every viscosity, it becomes clear that two flagella have a higher velocity only when the viscosity is increased sufficiently as can be seen in Table (1).

	1 flagellum		2 flagella	
	μ	σ	μ	σ
1.2 mPas	108.52	18.51	91.81	37.36
7 mPas	98.97	20.35	79.60	26.72
25 mPas	45.02	12.33	71.01	24.78

Table 1: The mean and standard deviation of the average path velocity µm/s per viscosity. The double flagellar sperm cell has a higher velocity than a single flagellar sperm cell for a high viscosity only.

Samples in three different viscosities were analyzed; $\eta = 1.2$ mPas, $\eta = 7$ mPas and $\eta = 25$ mPas. The mean and standard deviation of the wave variables are obtained for every viscosity using Equations (15) and (16). Figure (3) shows K_0 and A_0 and Figure (4) shows λ for sperm cells with one and two flagella.

It is to be seen that K_0 and A_0 decrease when the viscosity increases. The mean at a viscosity of $\eta = 1.2$ mPas with one flagellum is an exception to this. It has to be noted that only one sample with $\eta = 1.2$ mPas and one flagellum is being analyzed. For the wavelength λ, no relation is present regarding the viscosity. However, it is notable that the wavelength is the lowest for a viscosity of $\eta = 7$ mPas for both single flagellar sperm cells as double flagellar sperm cells.
In Table (2), the mean and standard deviation for every viscosity are shown for one flagellum and two flagella.

		μ	σ
1 flagellum	K_0 [rad/mm]	10.44	9.53
	A_0 [rad/mm]	8.16	4.47
	λ [µm]	75.10	44.74
2 flagella	K_0 [rad/mm]	6.85	6.78
	A_0 [rad/mm]	7.04	4.88
	λ [µm]	56.78	21.33

Table 2: Mean and standard deviation of the wave variables for a sperm cell with one and two flagella obtained from experimental data. The wave variables are lower for double flagellar sperm cells than for single flagellar sperm cells.

It is observed that the mean value for K_0 matches the value found by an earlier research [12]. Furthermore, it is noticed that the wave variables decrease for multiple flagella.

3.2 Implementation of regularized stokeslets for a single flagellum

Using the method of regularized stokeslets, the flow fields of multiple samples can be analysed.
In Figure (5), the flow field is depicted at an arbitrary moment in time around a flagellum with $K_0 = -3.1$ rad/mm, $A_0 = 8.9$ rad/mm and $\lambda = 48.82$ µm. It is to be seen that the fluid is approximately propelled along a trajectory from positive x-direction to the negative x-direction. On this trajectory, it passes the flagellum twice. Using the flow field as in Figure (5) for every moment in time, the average flow field can be obtained. It is known that the average flow field around a single flagellar sperm cell adheres to a repulsive field along the long axis of the sperm cell and attractive along the sides of the sperm, as can be seen in Figure (6). To get a clear view of the influence of the wave variables on the flow around a single flagellar sperm cell, different flow fields are obtained with varying wave variables. In turn, every wave variable will be iterated.

3.2.a A_0 iteration

First, the amplitude rise will be varied from $A_0 = 1$ rad/mm till $A_0 = 20$ rad/mm. In Figure (14), the different flow fields for $A_0 = 5$, 10, 15 and 20 rad/mm are shown. The mean flagellar curvature is $K_0 = 0$ rad/mm and the wavelength is $\lambda = 50$ µm. These flow fields are averaged over one beat cycle.
It is to be seen that the repulsive and attractive fields are present as depicted in Figure (6). Besides, the

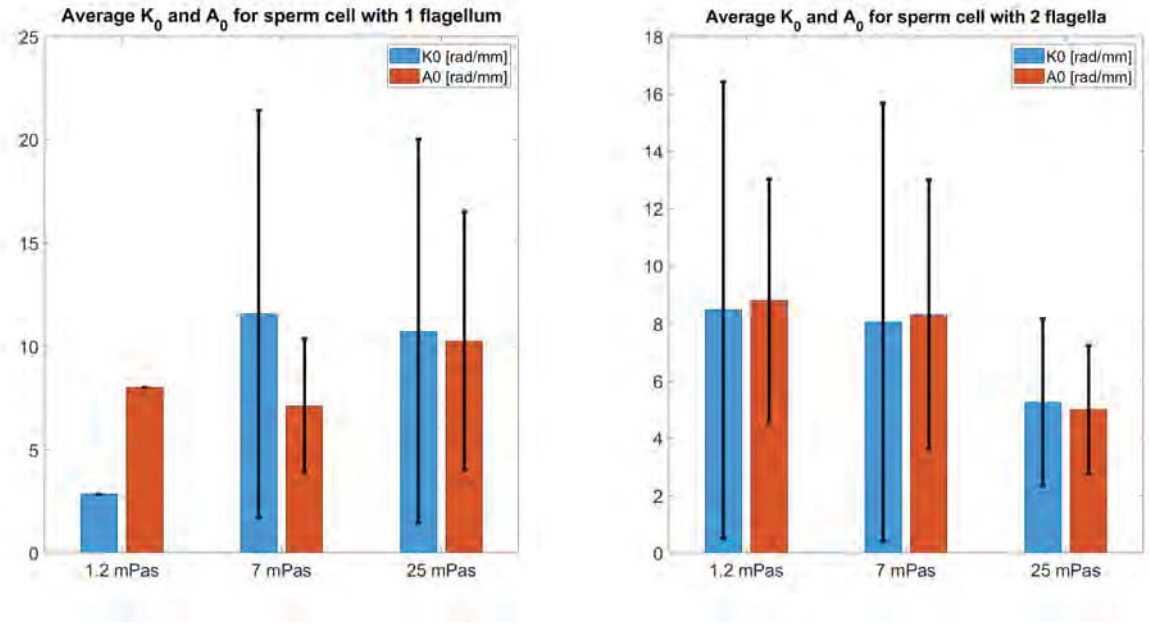

Fig. 3: The mean and standard deviation of K_0 and A_0 with varying viscosity for a sperm cell with one and two flagella. An increase in viscosity causes the mean flagellar curvature and the amplitude rise to decrease.

flow fields, also the velocity of the head can be determined. In Figure (7), the velocity is plotted against A_0. It is to be seen that the velocity increases as A_0 increases until $A_0 \approx 15$ rad/mm. From this point, the end of the flagella is slightly pointing in the positive x-direction. This decreases the propulsion of the flagellum and therefore, the velocity decreases. It has to be noted that this optimal value differs when the other wave variables are changed.

3.2.b K_0 iteration

The mean flagellar curvature will be varied from $K_0 = 0$ rad/mm till $K_0 = 20$ rad/mm with $A_0 = 10$ rad/mm and $\lambda = 50$ µm. Figure (15) shows the flow fields for $K_0 = 3$, 6, 9 and 12 rad/mm.

Again, the repulsive and attractive field is visible. However, the larger K_0, the less these fields are present. It is found that the velocity of the head in the x-direction decreases since the propulsion is redirected in the y-direction. For the same reason, the velocity in the y-direction increases. The resultant velocity $v = \sqrt{v_x^2 + v_y^2}$ is plotted in Figure (8). It is to be seen that the resultant velocity decreases as K_0 increases.

3.2.c λ iteration

Besides A_0 and K_0, the wavelength λ is of importance. The wavelength is varied from $\lambda = 10$ µm till $\lambda = 200$ µm. Furthermore, $K_0 = 0$ rad/mm and $A_0 = 10$ rad/mm. In Figure (16), the flow fields for $\lambda = 10$, 30, 50 and 70 µm are shown.

It is to be seen that the flow field in general, independent of the wavelength, behaves as depicted in Figure (6). However, when $\lambda \gtrapprox L_{tail}$, the flow field changes considerably. In Figure (9), the velocity in x-direction is plotted against the wavelength. This figure supports the above statement as the velocity is decreasing close after the wavelength is greater than the length of the flagellum.

From the above iterations, it can be concluded that the flow field around a single flagellar sperm cell always adheres to a repulsive flow along the long axis and an attractive flow field along the sides of the sperm cell as long as the wave variables K_0, A_0 and λ are not exaggerated.

3.3 Implementation of regularized stokeslets for two flagella

With the wave variables from the experimental data, the flow fields around double flagellar sperm cells can be obtained. In Section (3.1) it was observed that there appears to be a difference for double flagellar sperm cells between a low viscosity and a high viscosity. Therefore, the following section will take a look at a low viscosity situation as well as to a high viscosity situation.

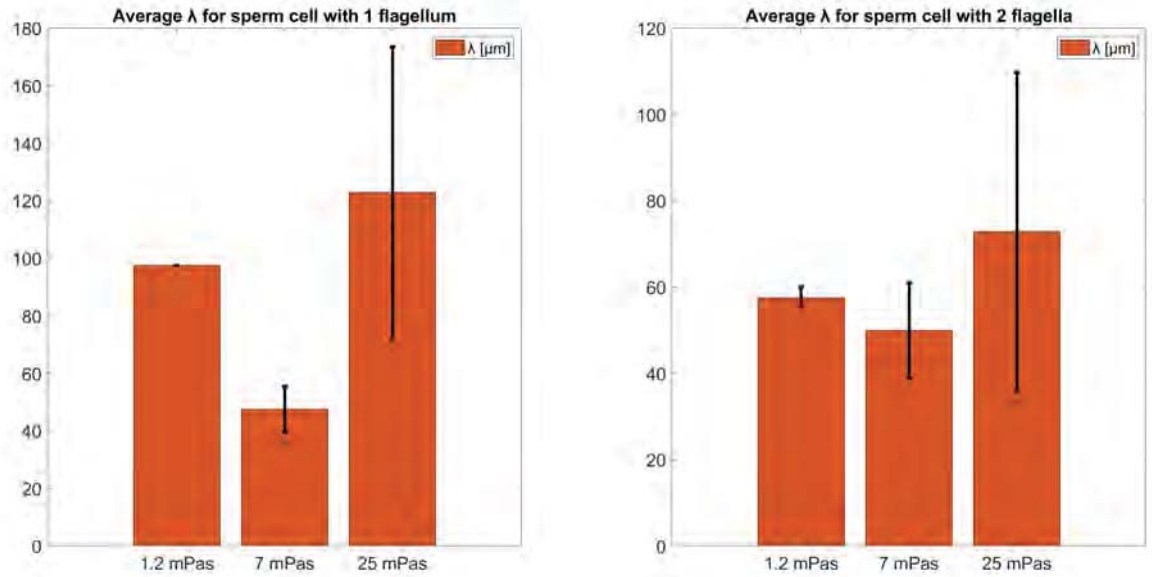

Fig. 4: The mean and standard deviation of λ with varying viscosity for a sperm cell with one and two flagella. No relation is to be seen between the viscosity and the wavelength. It is found that the wavelength for a viscosity of $\eta = 7$ mPas results in the lowest wavelengths.

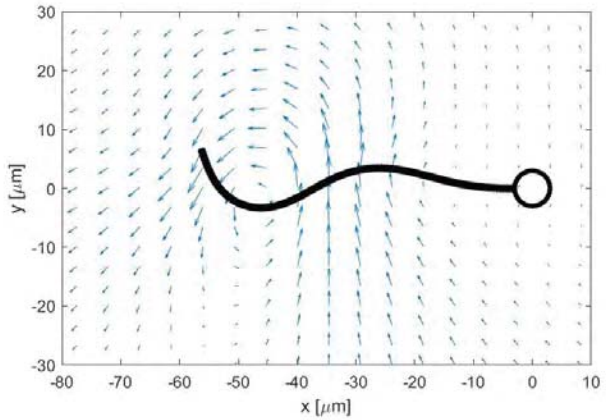

Fig. 5: The flow field around a single flagellar sperm cell at an arbitrary moment in time. The flow is propelled along the flagellum towards the negative x-direction. On its trajectory, the flow passes the flagellum multiple times.

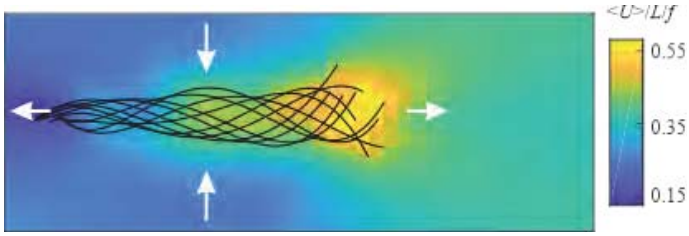

Fig. 6: The average flow field around a single flagellar sperm cell. Along the long axis, a repulsive force-field is present. Along the sides, an attractive field is present.

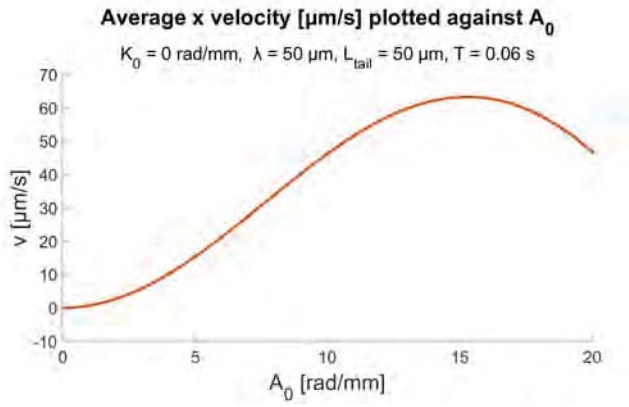

Fig. 7: Velocity in x-direction plotted against the amplitude rise A_0. The velocity in x-direction increases while K_0 increases until $K_0 \approx 15$ rad/mm. From there, the velocity decreases.

3.3.a Low viscosity

As a first example, a synchronized double flagellar sperm cell in a viscosity of $\eta = 7$ mPas is depicted in Figure (10). For the upper tail, $K_0 = -1.37$ rad/mm, $A_0 = 10.92$ rad/mm and $\lambda = 43.36$ μm. For the lower tail, $K_0 = 7.87$ rad/mm, $A_0 = 8.96$ rad/mm and $\lambda = 46.85$ μm. The length of both tails equals 60 μm. At the outermost sides of the sperm cells, an

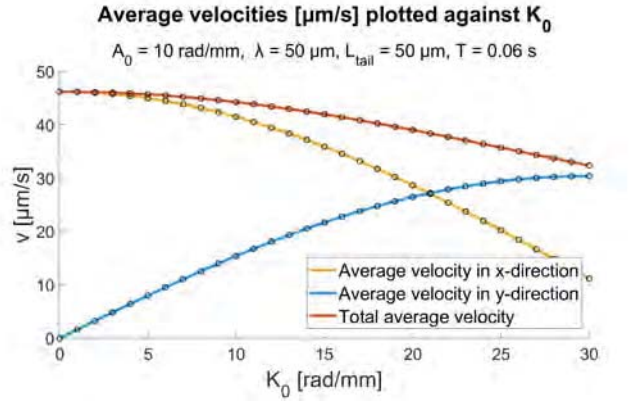

Fig. 8: The resultant velocity and velocity in x and y direction plotted against K_0. The velocity in x-direction decreases while the velocity in y-direction increases. The resultant velocity decreases as K_0 increases.

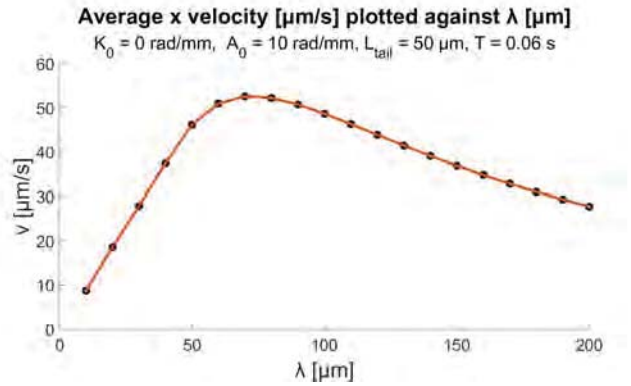

Fig. 9: The velocity in x-direction plotted against the wavelength λ. The velocity increase until $\lambda \approx L_{tail}$. Above this wavelength, the velocity starts to decrease.

attractive field is present, similar to the samples with one flagellum. This field is not present on the inner sides of the flagella because the flow is disturbed by the other flagellum. Within the beating flagella, it is to be seen that the fluids velocity in x-direction is amplified by the beating movement. In Figure (11), this amplification is clearly visible. Furthermore, the repulsive field can be distinguished in the flow field. At the end of both flagella, the flow is forced in the negative x-direction. At the head of the tail, this repulsive field is less visible, but still present.

The velocity of the sperm head is found to be 21.9545 µm/s in x-direction and 19.0613 µm/s in y-direction. The two flagella were modeled apart from each other to find their individual velocities. For the upper tail the velocity is found to be 45.5841 µm/s in x-direction and -2.6078 µm/s in y-direction. For

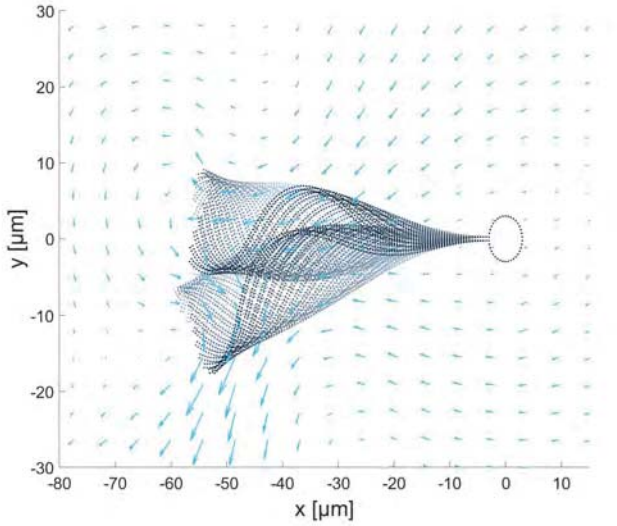

Fig. 10: The flow field around a synchronized double flagellar sperm cell in a low viscosity fluid.

the lower tail the velocity is found to be 40.3217 µm/s in x-direction and 13.7699 µm/s in y-direction. It is clear that the propulsion is not enhanced by adding both flagella together. In Figure (10), it is to be seen that the flow field is disturbing itself. At the lower tail, part of the flow is acting counterproductive leading to a lower flagellar propulsion. Evidently, the hydrodynamic interactions negatively influence the flagellar propulsion of this sperm.

In Figure (12a) the flow field is depicted at an arbitrary moment in time. It is to be seen that the fluid is propelled along a trajectory from the positive x-direction towards the negative x-direction. On this trajectory, the fluid passes the flagella multiple times. This behaviour is similar to the flow field of a single flagellar sperm cell as in Figure (5). Since the flagella beat in a synchronized pattern, this trajectory is allowed by both flagella. If the amplitude rise of the upper flagellum is inverted, the phase angle is moved with π and this trajectory is obstructed. In figure (12b), the corresponding flow field is depicted. Here, the trajectory of the fluid is being counterworked resulting in less propulsion during the complete beat cycle. It has to be noted that in reality, sperm cells are unlikely to swim like this. In actual existence, both flagella will adapt to each other because of the hydrodynamic interactions. This behaviour is not depicted here. From the above information, derived from experimental data, it is clear that a synchronized beat pattern has greater propulsion than a sperm cell

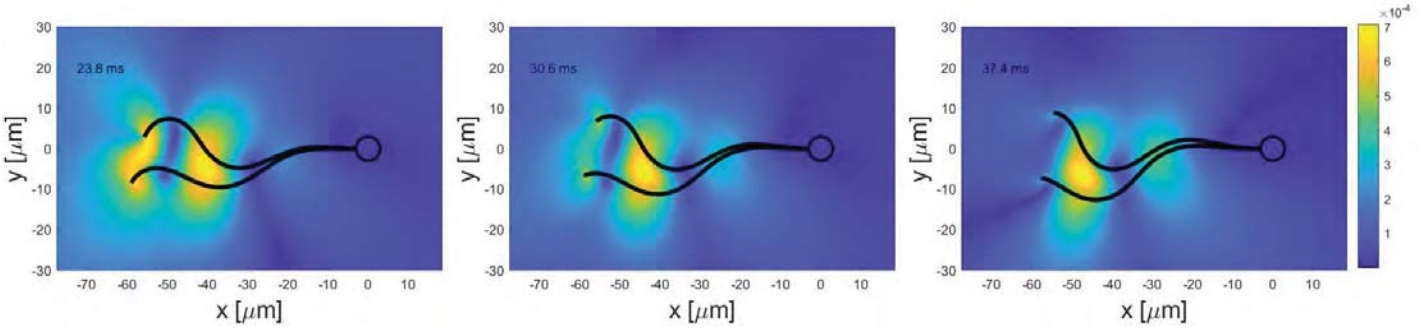

Fig. 11: The fluid velocity [m/s] at three sequential moments in time where the fluids velocity is amplified along the direction of the flagella.

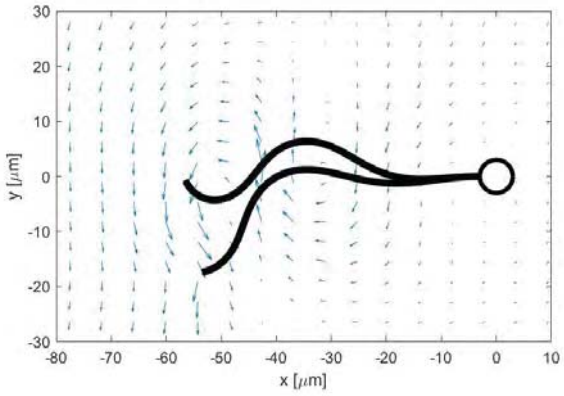

(a) The flow field around a synchronized double flagellar sperm cell at an arbitrary moment in time. The trajectory passes the flagella multiple times while being propelled form the positive x-direction to the negative x-direction.

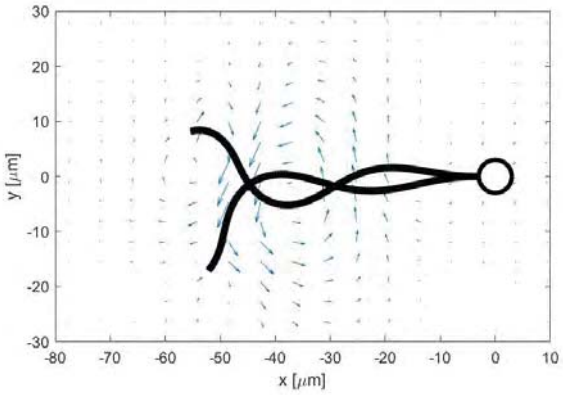

(b) The flow field around an out of phase double flagellar sperm cell at an arbitrary moment in time. The trajectory of the flow is a being disturbed and results in a vortex.

Fig. 12

with an out of phase beat cycle.

3.3.b High viscosity

It is known that the wave variables decrease for a higher viscosity. Therefore, the wave variables from an experimental sample in a viscosity of $\eta = 25$ mPas will be used. For the upper tail, $K_0 = 2.59$ rad/mm, $A_0 = 8.57$ rad/mm and $\lambda = 58.61$ μm. For the lower tail, $K_0 = 3.06$ rad/mm, $A_0 = 6.46$ rad/mm and $\lambda = 50.35$ μm. The length of both tails equals 60 μm. Figure (13) depicts the flow field around this synchronized sperm cell. The flow field again shows the repulsive and attractive field along the long axis and along the sides, respectively. Furthermore, it is noticed that the flow field is very similar to a single flagellar sperm cell with comparable wave variables (Figure (15), $K_0 = 6$ rad/mm, $A_0 = 10$ rad/mm and $\lambda = 50$ μm/s). Due to the relatively low wave variables, the waves are practically beating in the same pattern. For that reason, the flow field is well comparable with a single flagellar sperm cell. The velocity of the sperm head is found to be 29.8547 μm/s in x-direction and 0.13107 μm/s in y-direction. The two flagella were modeled apart from each other to find their individual velocities. For the upper tail the velocity is found to be 25.2201 μm/s in x-direction and 2.7317 μm/s in y-direction. For the lower tail the velocity is found to be 19.4975 μm/s in x-direction and 2.5045 μm/s in y-direction. The velocity of the double flagellar sperm cell is higher than both of the single flagellar sperm cells. That concludes that the hydrodynamic interaction between two flagella for this case increases the flagellar propulsion.

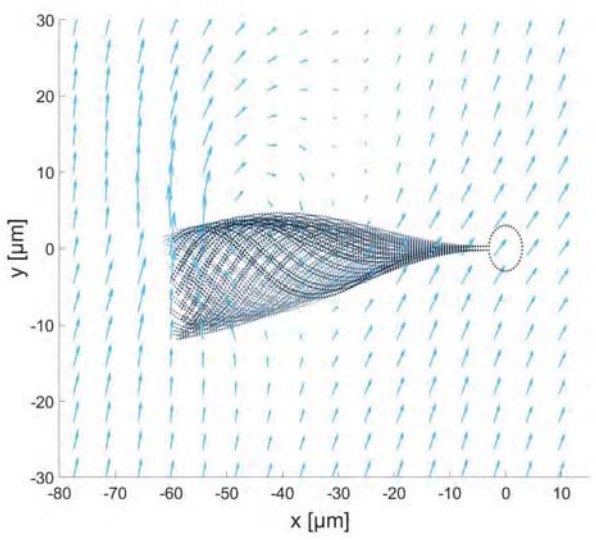

Fig. 13: The flow field around a synchronized double flagellar sperm cell in high a viscosity fluid.

It was found that the above examples are a good representation of the experimental samples. In a low viscosity, the double flagellar sperm cell appears to have a smaller flagellar propulsion compared to single flagellar sperm cells. For a high viscosity, the double flagellar sperm cells have a greater flagellar propulsion than the single flagellar sperm cells. In Section (3.1), it was found that for higher viscosities, the wave variables decrease. Furthermore, it is known that the velocity of a sperm cell is not dependent on the viscosity itself.
When the wave variables decrease, they are more similar for both flagella. It is observed that the flow field around the double flagellar sperm cell in a high viscosity is closely related to the flow field around a single flagellar sperm cell.
From this and the above, the conclusion can be made that the flagellar propulsion is increased when the wave variables of one tail are similar to the wave variables of the other tail.

4 CONCLUSION

The goal of this paper was to determine the effects of the hydrodynamic interactions between flagella on the traveling wave propulsion of the sperm cell. This was done by obtaining the wave variables K_0, A_0 and λ. With these variables, a statistical analysis could be performed. From this analysis, it was found that the averaged path velocity for single flagellar sperm cells is higher than for double flagellar sperm cells for low viscosities. For high viscosities, the double flagellar sperm cells have a higher averaged path velocity. It was also found that when the viscosity increases, the wave variables A_0 and K_0 decrease. This decrease is approximately linear. However, due to the low number of analyzed experimental data, this can not be concluded with certainty. Finally, the wave variables for double flagellar sperm cells are found to be lower than the wave variables for single flagellar sperm cells.
After the statistical analysis, the influence of the wave variables on the flowfield around a single flagellum is studied. It is found that the wave variables do not influence the behaviour of the flow field around the flagella as long as they are not exaggerated. For the wave variables obtained from the experimental data, the flow field will always consist of a repulsive field along the long axis and an attractive field along the sides of the sperm cell.
Finally, the effect of having two flagella instead of one is studied. For double flagellar sperm cells, it is found that the hydrodynamic interactions decrease the flagellar propulsion when the wave variables of one tail are not similar to the other. This is often the case in low viscosity fluids. For high viscosity fluids, the wave variables are generally smaller and therefore naturally more similar. With similar wave variables, the hydrodynamic interactions increase the flagellar propulsion.

In further research, it is advised to possess more analyzed samples. With more data, the averaged wave variables and velocities in Section (3.1) will be more accurate.
It is observed that the wave variables decrease when having two flagella instead of one. Understanding this observation would be a valuable acquisition regarding the understanding of multiple flagellar propulsion.

ACKNOWLEDGEMENTS

I would like to thank I.S.M. Khalil for guiding me throughout my research and encouraging me about the subject. I thank K. Zhang for helping me throughout my research with various problems. I thank M.W. Hoppenreijs for providing feedback and sharing thoughts. I thank D.H. Ramadhin, J. Dias, Y. Le Gars and Z. Wang for analyzing experimental data.

REFERENCES

1. Karsten König, *Minimally invasive medicine*, 202–205, Springer Berlin Heidelberg, Berlin, Heidelberg, (2009).
2. M. Sitti, Hakan Ceylan, Wenqi Hu, J. Giltinan, Mehmet Turan, S. Yim, and E. Diller, Biomedical applications of untethered mobile milli/microrobots, *Proceedings of the IEEE*, (2015), 103:205–224.
3. G. J. Hancock and Maxwell Herman Alexander Newman, The self-propulsion of microscopic organisms through liquids, *Proceedings of the Royal Society of London. Series A. Mathematical and Physical Sciences*, (1953), 217(1128):96–121.
4. Ajay Vikram Singh, Mohammad Hasan Dad Ansari, Mihir Mahajan, Shubhangi Srivastava, Shubham Kashyap, Prajjwal Dwivedi, Vaibhav Pandit, and Uma Katha, Sperm cell driven microrobots—emerging opportunities and challenges for biologically inspired robotic design, *Micromachines*, (2020), 11(4).
5. B. M. Friedrich, I. H. Riedel-Kruse, J. Howard, and F. Jülicher, High-precision tracking of sperm swimming fine structure provides strong test of resistive force theory, *Journal of Experimental Biology*, 04 2010, 213(8):1226–1234.
6. I. Riedel-Kruse, A. Hilfinger, J. Howard, and F. Jülicher, How molecular motors shape the flagellar beat, *HFSP Journal*, (2007), 1:192 – 208.
7. D H Ramadhin, Flagellar propulsion of paired bull spermatozoa, (2021).
8. B Y J Gray and G J Hancock, The Propulsion of Sea-Urchin Spermatozoa, *Journal of Experimental Biology*, (1955), 32(4):802–814.
9. Ricardo Cortez, The method of regularized stokeslets, *SIAM Journal on Scientific Computing*, (2002), 23(4):1204–1225.
10. Ricardo Cortez, Lisa Fauci, and Alexei Medovikov, The method of regularized Stokeslets in three dimensions: Analysis, validation, and application to helical swimming, *Physics of Fluids*, (2005), 17(3):1–15.
11. Veronika Magdanz, Jacopo Vivaldi, Sumit Mohanty, Anke Klingner, Marilena Vendittelli, Juliane Simmchen, Sarthak Misra, and Islam S. M. Khalil, Impact of segmented magnetization on the flagellar propulsion of sperm-templated microrobots, *Advanced Science*, (2021), 8(8):2004037.
12. Islam S. M. Khalil, Veronika Magdanz, Juliane Simmchen, Anke Klingner, and Sarthak Misra, Resemblance between motile and magnetically actuated sperm cells, *Applied Physics Letters*, (2020), 116(6):063702.

A APPENDIX

On the following pages, Figure (14), (15) and (16) are to be seen.

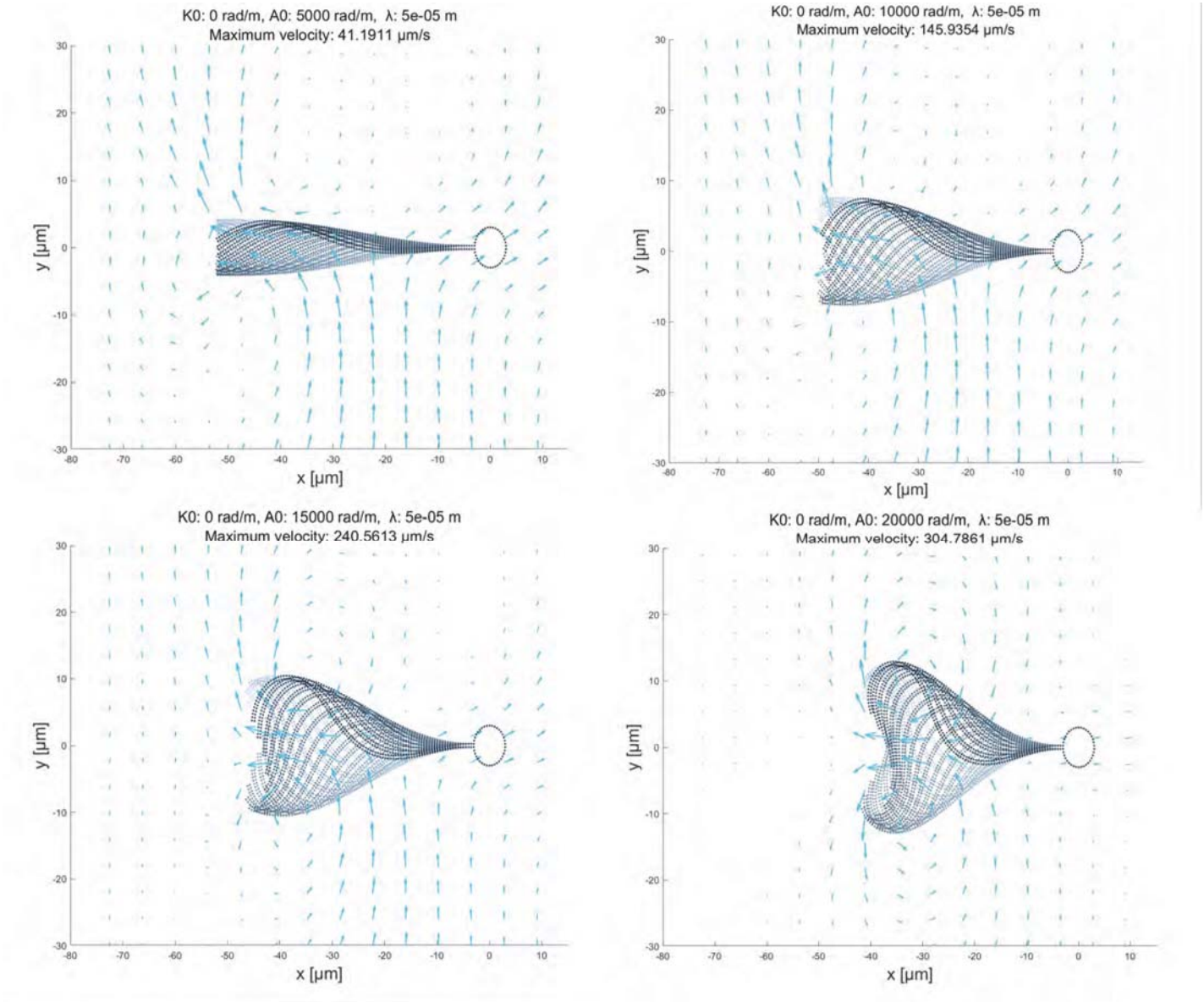

Fig. 14: Nondimensionalized flow fields of a single flagellar sperm cell with $A_0 = 5,\ 10,\ 15\ \&\ 20$ rad/mm. $K_0 = 0$ rad/mm, $\lambda = 50$ μm, $T = 0.06\ s$, $\eta = 7$ mPas and the length of the tail equals 50 μm.

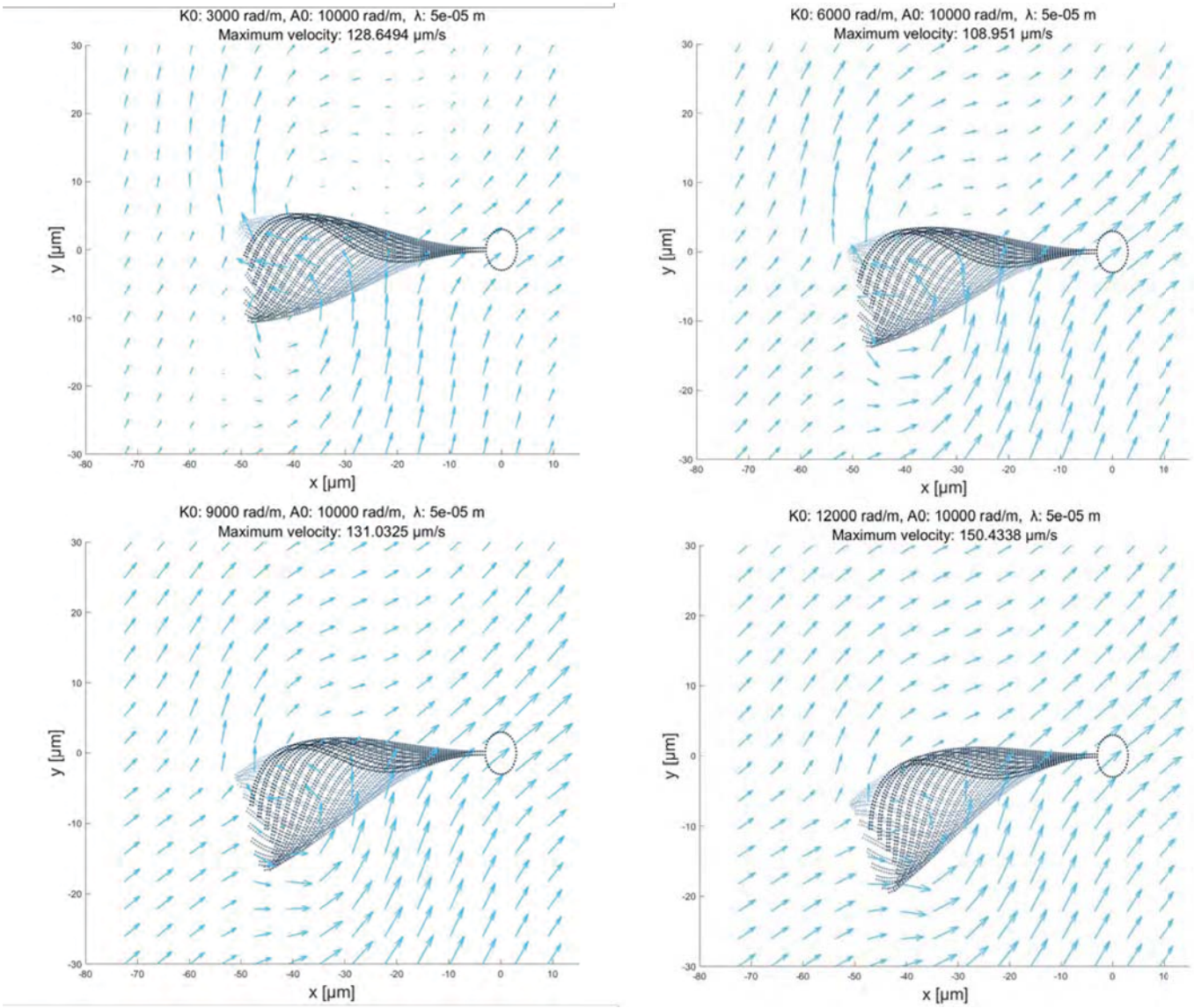

Fig. 15: Nondimensionalized flow fields of a single flagellar sperm cell with $K_0 = 3,\ 6,\ 9\ \&\ 12$ rad/mm. $A_0 = 10$ rad/mm, $\lambda = 50$ µm, $T = 0.06\ s$, $\eta = 7$ mPas and the length of the tail equals 50 µm.

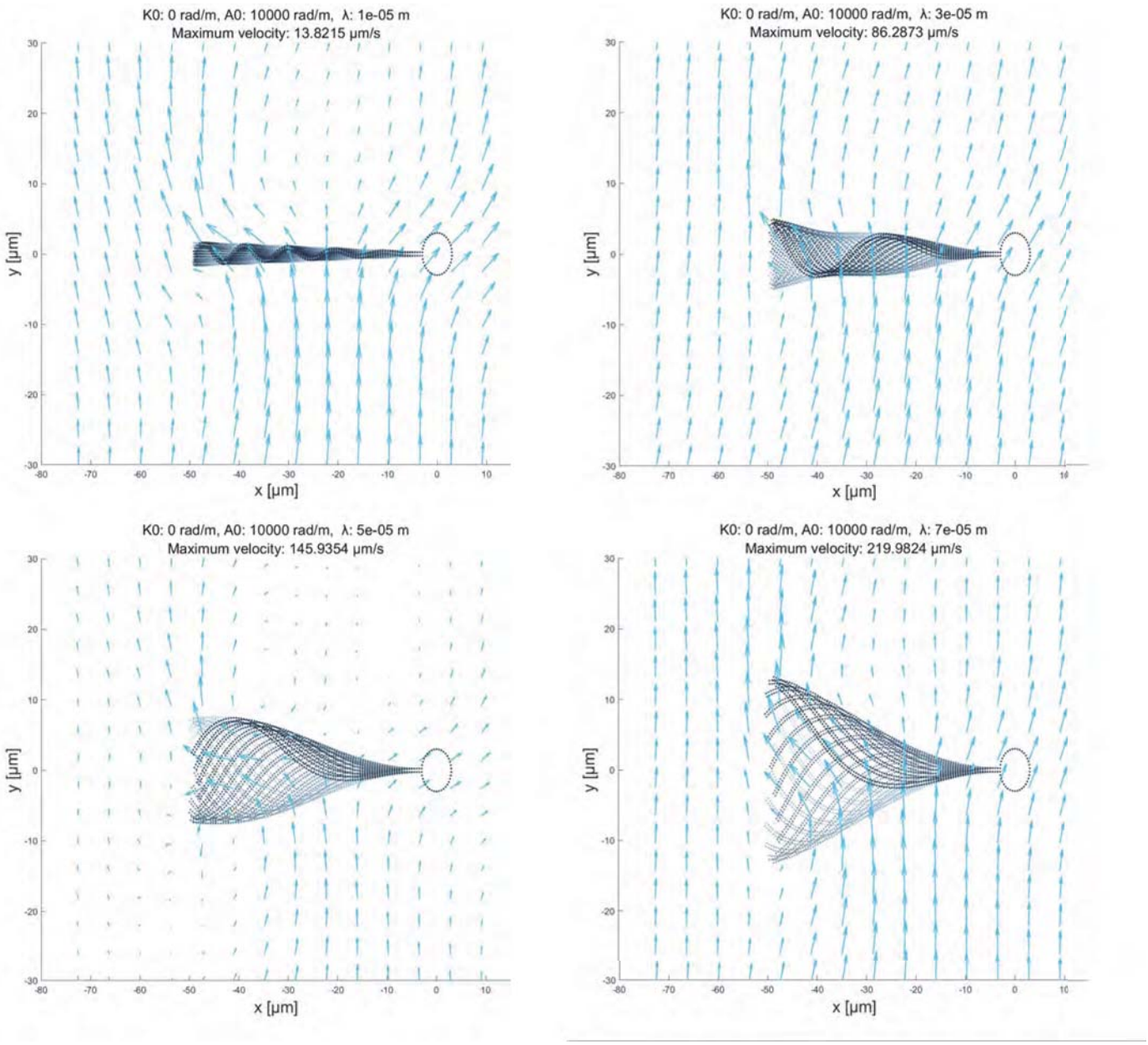

Fig. 16: Nondimensionalized flow fields of a single flagellar sperm cell with $\lambda = 10, 30, 50$ & 70 μm. $A_0 = 10$ rad/mm, $K_0 = 0$ rad/mm, $T = 0.06$ s, $\eta = 7$ mPas and the length of the tail equals 50 μm.